University of Birmingham
School of Physics and Astronomy

Y4 Project

Bayesian Hierarchical Modelling of Helium Signatures in Red Giant Stars

MSci Project Report

Daniel Alexander Williams

ID: 1524438
28th March 2019

Project partner: Joshua Cardrick
Supervisor: Dr. Guy Davies

Abstract

The spread of helium enrichment throughout stars in the galaxy and wider universe is poorly understood, despite its abundance as an element. One method by which abundance can be inferred is using asteroseismology to study the 'helium glitch' region in Red Giant stars. In contrast to previous studies, we aim to apply a Hierarchical Bayesian Model to a large set of RGB stars in the APOKASC catalogue, to leverage the power of population statistics in order to decrease the uncertainty of our results. We develop an updated set of constrained power laws for asteroseismic parameters with an improved glitch model, and discover using hierarchical analysis that the spread of helium abundance does not appear to be uniform across different populations of stars, with potential impacts on our understanding of stellar enrichment theory.

Keywords: Asteroseismology, Bayesian Statistics, Hierarchical Modelling, HBM, Stars: Helium Glitch, Enrichment

Word Count: 7653

Contents

1 Introduction

Helium is the second most abundant element in the universe, however our understanding of the spread of its abundance amongst stars is comparatively poor. The helium content within stars cannot be easily measured using direct means, partly since the surface layer is not representative of the internal make-up.[1] This uncertainty affects our wider understanding of stellar evolution, since the helium mass fraction Y is currently either fixed between models or made a follow a simplistic relationship from the measured metallicity.

Asteroseismology however provides a novel tool with which we can probe inside the interiors of stars, by looking at how the presence of Helium has an impact on the way sound propagates through the internal strata of each star. Recent investigations using this method such as by Vrard et al. (2015)[2] have looked at a feature known as the 'Helium Glitch' in evolved Red Giant Branch (RGB) stars, however they concluded that it is very difficult to ascertain a measure of the helium abundance on a star-by-star basis. Using a similar analytical model,

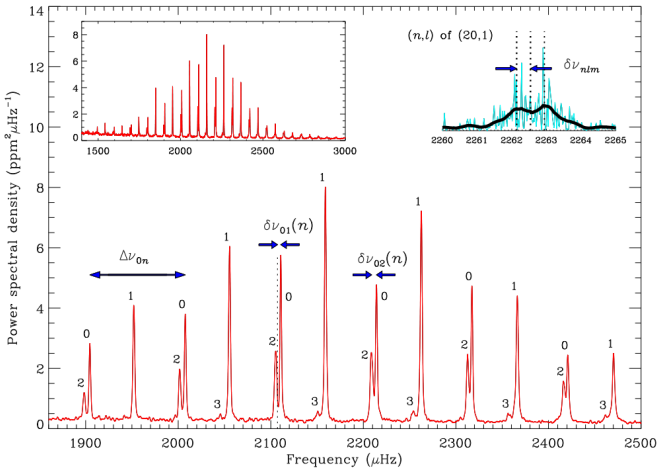

Figure 1: *An example asteroseismic spectrum showing the overall power envelope of the signal, and containing individual mode oscillations at regular spacings. The location of peak power is denoted ν_{max}, and large frequency spacing $\Delta\nu$.*

we have built upon this previous work by introducing a hierarchical Bayesian model (HBM), a powerful tool for inference that allows us to leverage the statistics of a large population to obtain a more robust measure of the spread of helium abundance amongst stars.

2 Theory

2.1 Asteroseismology

Unlike historical direct methods of stellar observation, such as spectroscopy, asteroseismology looks at the impact of trapped sound waves within the cavity provided by a star, and their impact on subtle changes in the brightness of the stellar surface. In cool stars, there are two predominant types of oscillation, pressure and gravity modes. Low-mass stars that have exhausted their core's nuclear fuel supply evolve off the main sequence onto the Red Giant Branch (RGB); in these stars modes of mixed character may also occur. Such stars are known as Solar-like oscillators since they share a common internal structure with the sun: an inner radiative zone with an outer convective envelope.

Pressure modes originate from pressure gradients within the star that provide a restoring force to any pertubation. They are described using two parameters: n the overtone number (radial order); and l, the angular degree. Observations of solar-like oscillators are most sensitive to oscillations of higher radial order and lower angualar degree, whose frequencies are

described by [3]

$$\nu_{nl} \simeq \Delta\nu \left(n + \frac{l}{2} + \varepsilon \right) - \Delta\nu^2 \left\{ \frac{A\left[l\left(l+1\right)\right] - B}{\nu_{nl}} \right\} \tag{1}$$

where ε relates to the boundary conditions of the oscillation cavity with A and B as undefined coefficients. The large asymptotic frequency spacing $\Delta\nu$, is described by

$$\Delta\nu = \left(2 \int_0^R \frac{dr}{c} \right)^{-1} \tag{2}$$

which is the equivalent to the inverse of the acoustic diameter of the star, the time taken for sound to traverse the stellar diameter at adiabatic sound speed c. The regular spacing between modes of identical angular degree l can also be defined directly by

$$\Delta\nu_{n,l} = \nu_{n,l} - \nu_{n-1,l} \approx \Delta\nu. \tag{3}$$

with each mode manifesting as a peak in the power spectrum of the star, as seen in Figure 1 – we will solely be considering the radial modes ($l = 0$) of oscillation, which are the only modes that probe through the entire acoustic depth of the star.

Frequencies of oscillations can be more informatively represented in an Échelle diagram. The modulo of the oscillation frequencies is taken with respect to $\Delta\nu$, with the results that modes of similar angular degree roughly line up (only for pressure modes), as seen in Figure 2. More subtle features can also be seen such as a mild curvature, and also a low-amplitude oscillation, which is the feature of interest.

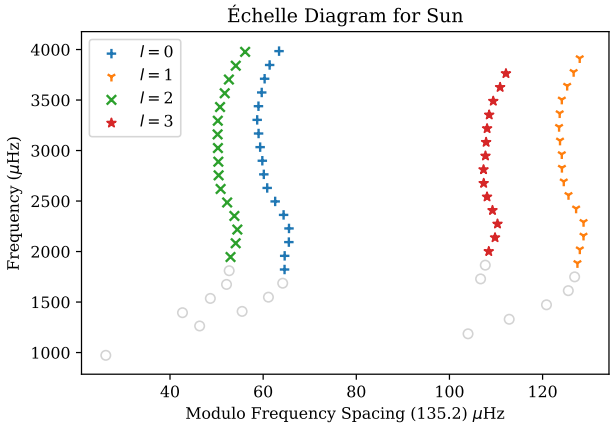

Figure 2: *An Échelle Diagram of the Sun, constructed using data from the Birmingham Solar Oscillations Network (BiSON). Note how modes of the same angular degree l roughly line up.* [4,5]

For a more comprehensive review and introduction to Asteroseismology, please refer to the summary article by Chaplin et Miglio (2012). [3]

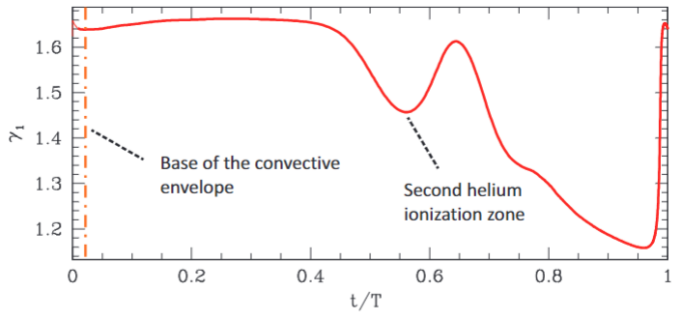

Figure 3: *Behaviour of adiabatic exponent γ_1 with respect to acoustic radius t in a RGB star, showing the pronounced dip around the location of the HeII ionisation region.* [6]

2.2 The Helium Glitch

The regular spacing of pressure mode frequencies in stars can be perturbed by changes to the local stellar structure; these are known as 'acoustic glitches'.

In the outer regions of main sequence and evolved red giant branch (RGB) stars, helium can be singly ionised into the He^+ species, known confusingly as HeII. The process of ionising helium extracts from energy radiating out of the star. In order for hydrostatic equilibrium to be maintained, density within this region increases. This change is demonstrated by a parameter known as the first adiabatic exponent γ_1, a differential measure of the structure of a star given

$$\gamma_1 = \left(\frac{d \ln P}{d \ln \rho} \right)_s \tag{4}$$

where P and ρ are pressure and density at constant entropy s. Figure 3 shows the behaviour of the adiabatic exponent throughout a RGB star. A sharp change in the value of γ_1 impacts the local sound propagation speed c thus

$$c^2 = \frac{\gamma_1 P}{\rho} \tag{5}$$

which in turn causes a small shift of the eigenfrequencies for the lower order (in l, n) oscillations. [7,8] This shift can be quantitatively represented by the previously undefined term A in equation 1, which can be shown as

$$A = \frac{1}{4\pi\Delta\nu} \left[\frac{c(R)}{R} - \int_0^R \frac{dc}{dr} \frac{dr}{r} \right] \tag{6}$$

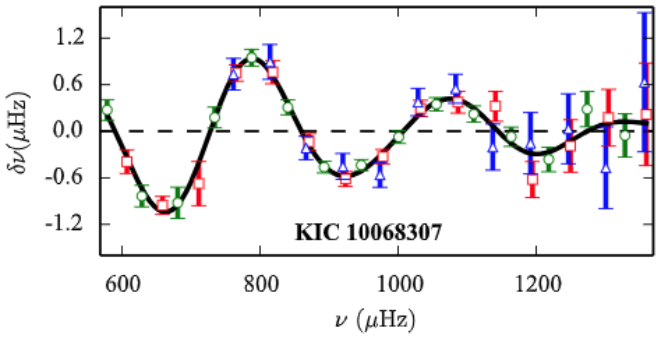

Figure 4: *The characteristic signal caused by the helium glitch, with radial $l = 0$ modes coloured in red.*[9]

noting the dependence on the changing value of c.

The appearance of the helium glitch with increasing frequency follows a decaying sinusoidal signal, as seen in Figure 4, whose shape can be described by two effects. The sinusoidal element arises from the changing position of the nodes of the radial pressure modes. As radial order n increases, these nodes move in and out of the radial extent of the HeII ionisation region, causing a periodic change in the sensitivity of successive modes. As the radial modes reach higher orders in n, the acoustic wavelength associated with a particular modal oscillation becomes shorter. Eventually, if this wavelength becomes comparable to or smaller than the radial extent of the glitch region, the modes become desensitised to the local change in adiabatic sound speed, causing the amplitude of the glitch to exponentially decay at higher frequencies.[10,11]

2.3 Hierarchical Bayesian Models

In order to take advantage of population statistics, it was necessary to construct a model that not only could fit the individual glitch parameters for each star, but provide us with a measure of the spread of these parameters across the whole population; this is where using a HBM becomes invaluable.

A hierarchical model has multiple levels of inferred parameters. Each individual star is described by a set of latent parameters $\vec{\theta}$ that provide the modelled value of the variable x. In our model x represents the frequencies of the oscillations, whereas $\vec{\theta}$ includes the amplitude and period of the glitch oscillation. The model only becomes hierarchical however once we impose the condition that latent parameters themselves can have their distributions described with population-related parameters, such that $\vec{\theta_i}|\mu \sim \mathrm{N}(\mu, \sigma_\mu)$ – there are no restrictions on the

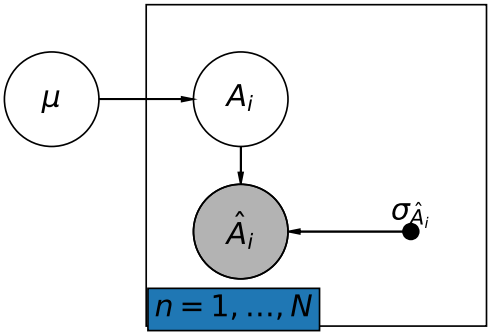

Figure 5: *A very simple probabilistic graphical model. Hyperparameters are represented by μ on the left, which inform the set of latent parameters A_i. Observed data and associated errors are shown by the shaded circle and dot respectively, whilst arrows represent the flow of information for N data points.*

number of hyperpriors and hierarchical levels. Using Bayes' Theorem, the posterior is given by

$$\mathrm{p}(\vec{\mu}, \vec{\theta}|x_i) \propto \mathrm{p}(x_i|\vec{\mu}, \vec{\theta})\mathrm{p}(\vec{\theta}, \vec{\mu})\mathrm{p}(\vec{\mu}) \tag{7}$$

where the right-hand terms are the likelihood, prior and hyperprior distributions.

A HBM can very quickly become rather complex and confusing to understand; one method that can be used to diagramatically show the link between parts of a model is in a 'probabilistic graphical model', an example of which is shown in Figure 5.

3 Procedure

3.1 Constructing the Model

To construct our model, we chose to adapt the helium glitch model previously explored by Vrard,[2] but with the addition of an decaying exponential term, which hadn't previously been investigated. We define $\Delta n = n - n_{max}$ and

$$n_{max} = \frac{\nu_{max}}{\langle \Delta\nu \rangle} - \varepsilon \tag{8}$$

where ε is normally valued between 0-1 and related to boundary conditions, and ν_{max} is the frequency with greatest signal strength, as seen in Figure 1. This leads us to the overall glitch model

$$\nu_{n,0} = \langle \Delta\nu \rangle \left[n + \varepsilon + \frac{\alpha}{2}(\Delta n)^2 + \frac{\mathcal{A}\mathcal{G}}{2\pi} \sin\left(\frac{2\pi(\Delta n)}{\mathcal{G}} + \phi \right) e^{-\frac{\Delta n}{\tau}} \right] \tag{9}$$

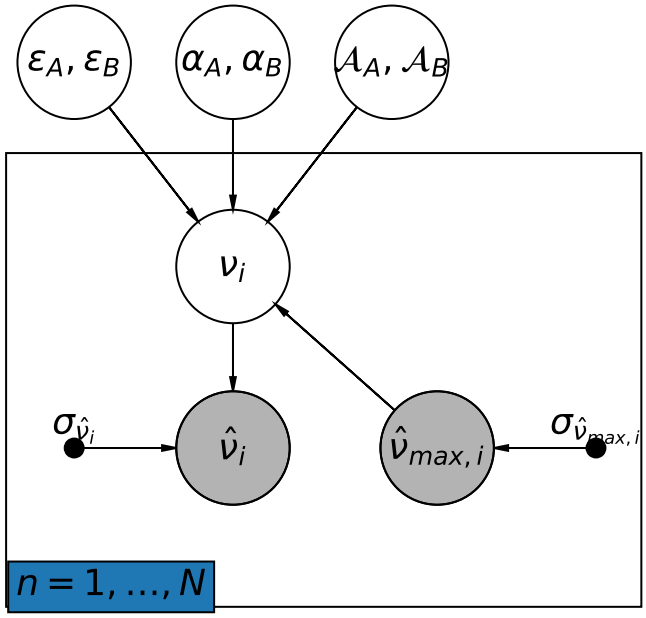

Figure 6: *A probabilistic graphical model depicting the flow of information in our hierarchical Bayesian model. The six hyperparameters are grouped above, whose information provided to the latent parameters in order to calculate the radial mode frequencies for each star. The latent parameters are also informed by the observed value of ν_{max} for each star.*

where α measures the curvature on the Échelle diagram; $\mathcal{A}$ and $\mathcal{G}$ are expressed in units of $\langle\Delta\nu\rangle$, representing amplitude and period respectively. ϕ is simply the phase and τ the dimensionless decay constant.

Given the model described above, we introduced a series of hyperparameters, following the relations:

$$\varepsilon = \varepsilon_A + \varepsilon_B \ln(\langle\Delta\nu\rangle) \tag{10}$$

$$\alpha = \alpha_A \langle\Delta\nu\rangle^{-\alpha_B} \tag{11}$$

$$\mathcal{A} = \mathcal{A}_A \langle\Delta\nu\rangle^{-\mathcal{A}_B} \tag{12}$$

whose purpose was to allow us to infer information about the population statistics of the sample data, by means of fitting a power law.

Following on from the example in Figure 5, we can construct a probabilistic graphical model to represent our fully defined HBM, shown in Figure 6.

3.2 Implementation using Stan

To implement our hierarchical model, we made use of the probabilistic statistical language `Stan`,[12] which offers significant computational advantages for Bayesian inference through the use of a Hamiltonian Monte Carlo (HMC) sampler. Stan makes use of a particular implementation of the HMC method known as the 'no U-turn' sampler. In short, the effect of this is that as an individual chain explores the posterior parameter space, it has an associated momentum. This acts as an effective mechanism to prevent the sampler returning to regions of the posterior it has already explored with lower probability. This helps to increase the speed of convergence, particularly in our context of fitting a large sample of stars simultaneously.

We interfaced with Stan using the python package `PyStan (v2.18.0.0)`. In order to obtain appropriate convergence of the individual chains, measured using the parameter $\hat{R}$, two runs of the sampler were performed. First, a simplified version of the model seen in Equation 9 was run, excluding the exponential decay. This was run for 8000 iterations across four chains, discarding the first half as burn-in. The results from this initial run were parsed into the complete model incorporating tau, providing much improved starting values for the sampler. 20000 iterations were performed to achieve the final results.

3.3 Data

Our sample of stars is derived from asteroseismic data from the first *Kepler* mission, using the APOKASC catalogue[13]. This comprises of a large number of evolved stars in the RGB and Red Clump (post-RGB) phases of evolution. RGB stars are ideal for our study into the helium glitch since these stars have very deep convective envelopes. The large separation between the glitch region and the base of the convective zone (BCZ) is beneficial since the latter also can cause a change to γ_1 that would otherwise interfere with the observed signal. We used the evolutionary classification scheme devised by Elsworth et al. (2017)[14] to distinguish the different classes of stars in our sample.

The original catalogue contained 1212 for which there was full information relating to induvidual frequencies and ν_{max} values. We calculated the average frequency spacing using the first frequency spacing, as described in equation 3. This differs from methods taken in previous studies such as by Vrard et al. (2017)[2] and Broomhall et al. (2014)[15] where the second frequency spacing, defined

$$\Delta_2\nu_{n,l} \equiv \nu_{n-1,l} - 2\nu_{n,l} + \nu_{n+1,l} \tag{13}$$

was used. Among reasons cited for their choice included introduction of additional fitting parameters

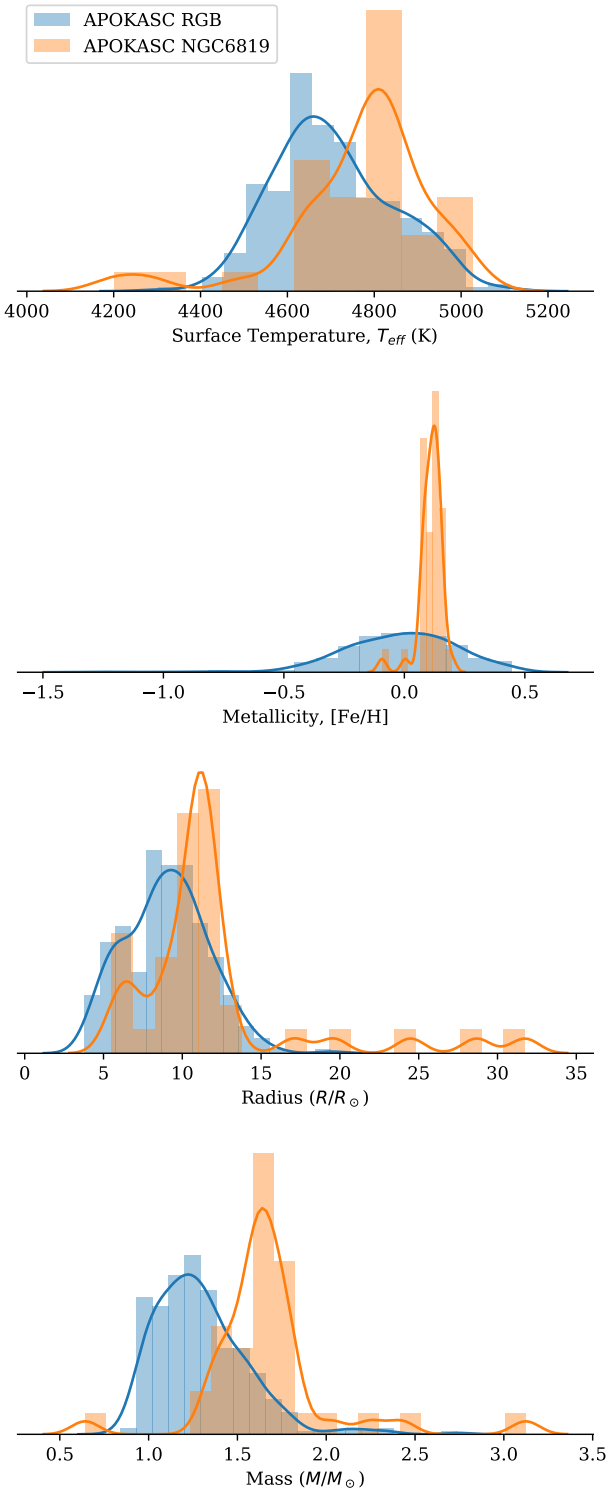

Figure 7: *Histograms showing the distribution of surface temperatures and metallicities between the field stars of the APOKASC catalogue and stars from the cluster NGC6819. NGC6791 has not been included in these plots due to insufficient numbers of stars in the sample having available values.*

into the model due to smoothly varying non-adiabatic processes – we believe the use of a hierarchical model across the whole population overcomes this issue, and also reduces the risk of autocorrelation and propagation of uncertainties compared to the second frequency differences.

Applying the Elsworth scheme located 422 RGB stars and 603 Red Clump stars. The remaining stars were classified under other stages of evolution (e.g. ABG) or unclassified and were not analysed futher. Following the initial run through Stan, the quality of the converged fits was checked for nonsensical parameter values. Any errant stars were prohibited from being analysed by the final model incorporating tau, to prevent these results being spoilt. This provided us with 396 RGB and 340 RC stars whose parameters were well converged. These were finally cross-referenced with the updated second APOKASC catalogue[16] in order to obtain quantities such as effective temperature and metallicity.

In addition to field stars, data was also available from the clusters NGC6819 and NGC6791, which were chosen for their unusual status as aged open clusters – this provides an advantage since most stars should have the same starting metallicity and initial helium. The data from the clusters was treated to a similar reduction method as previously described for the field stars.

Figure 7 shows how the difference between the general catalogue stars and those which are members of the cluster. NGC6819 is seen to have a marginally higher average set of $T_{\rm eff}$, although as would be expected for a cluster, the range of metallicities is much lower.

4 Stellar Models

To allow comparisons to be made with the observed oscillation frequencies, a grid of stellar models was produced using the evolutionary code Modules for Experiements in Stellar Astrophysics (MESA, `v10108`[17,18,19,20]). Models were varied over three parameters: mass M, initial helium abundance Y_0 and initial metallicity [Fe/H].

Table 1: Stellar Model Parameters

M	0.8	1.0	1.2	1.4	1.6	1.8
Y_0	0.24	0.26	0.28	0.32	0.36	0.40
[Fe/H]	-1.2	-0.6	-0.3	-0.15	+0.0	+0.15

The selected mass and metallicity ranges roughly matched the spread in the provided data, whilst higher values for Y were used to test for highly enriched scenarios. Each model was evolved along the RGB until a radius of approximately $32R_{\odot}$ ($\log R = 1.5$).

Radial pressure modes ($l = 0$) were calculated using GYRE (`v5.1`)[21,22] at intervals along the RGB for each model. Oscillation frequencies for the clusters NGC6791 and NGC6819 were accordingly produced using the oscillation code 'Asteroseismic Inference on a Massive Scale' (AIMS)[23,24,25].

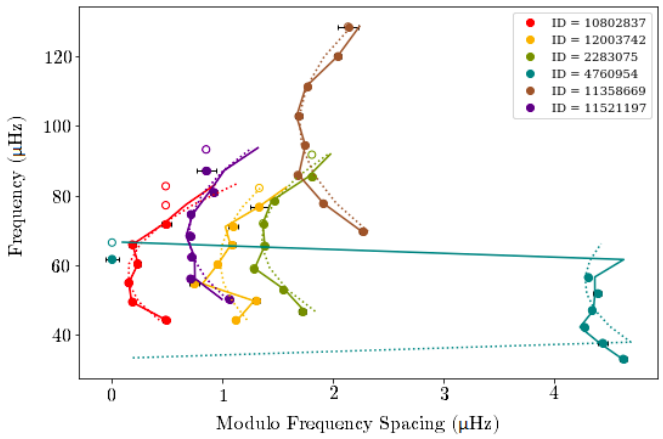

Figure 8: *An Échelle diagram showing the resulting frequency fits from running stars through the hierarchical model on a random sample of stars. The observed frequencies for each stars are in coloured dots, with the solid line the prediction for the glitch. The smooth dotted line is a comparison to show a fit with no glitch present (ie* $\nu_{n,l} = \Delta\nu\left[n + \varepsilon + 0.5\alpha\left(\Delta n\right)^2\right]$*), whilst the hollow points are simply placeholders so each star has the same number of modes; the model is not influenced by these.*

5 Results

Figure 8 shows the quality of the converged model on a number of stars within the sample. This shows that our chosen model described in equation 9 was sensibly motivated and could be applied to a larger sample of stars.

The feedback provided by the initial values of the hierarchical parameters allowed us to provide informative priors on the full model that would prevent the parameters exploring any regions which did not correspond to physical results. For example, the hyperparameters A_A and A_B had $\mathcal{U} \sim (0, 5)$ imposed on them, where $\mathcal{U}$ is a uniform distribution, as it was understood the amplitude of the glitch follows a decaying power law previously described in equation 12.

Using the newly informed priors and hyperpriors, the results for the asymptotic hierarchical relations are shown in Table 2. These results have also been illustrated in Figure 9, with each model parameter plotted against the average frequency spacing $\langle\Delta\nu\rangle$, and subtle error bars added for clarity. This allows the power laws derived using the HBM to be illustrated, showing the different laws derived using both RGB and RC stars.

Figures 10-11 provide similar plots, but for analysis of the clusters NGC6891 and NGC6719 respectively. To provide an easier means of comparison between the cluster and field data, the field stars have been plotted as a background – any unusual features in the cluster results then become more apparent, as seen in Figure 11.

Having plotted each parameter against $\langle\Delta\nu\rangle$, it is also useful to look at the set of joint-probability correlation plots for the glitch parameters, seen in Figure 12. In addition to the set of individual histograms, a colour map has been provided to see which parameters (if any) have a dependence upon the surface temperature T_{eff}.

Table 2: Asymptotic parameters relations.

Parameter	RGB	Red Clump
ε	$(-0.227 \pm 0.005) + (0.191 \pm 0.003)\ln\langle\Delta\nu\rangle$	$(-0.373 \pm 0.015) + (0.242 \pm 0.009)\ln\langle\Delta\nu\rangle$
α	$(0.030 \pm 0.001)\langle\Delta\nu\rangle^{-0.467\pm0.025}$	$(0.027 \pm 0.002)\langle\Delta\nu\rangle^{-0.484\pm0.053}$
$\mathcal{A}$	$(0.089 \pm 0.005)\langle\Delta\nu\rangle^{-0.767\pm0.028}$	$(0.115 \pm 0.007)\langle\Delta\nu\rangle^{-0.802\pm0.040}$
$\mathcal{G}$	3.08 ± 0.88	
ϕ	$-1.9 + 1.5\ln\langle\Delta\nu\rangle$	

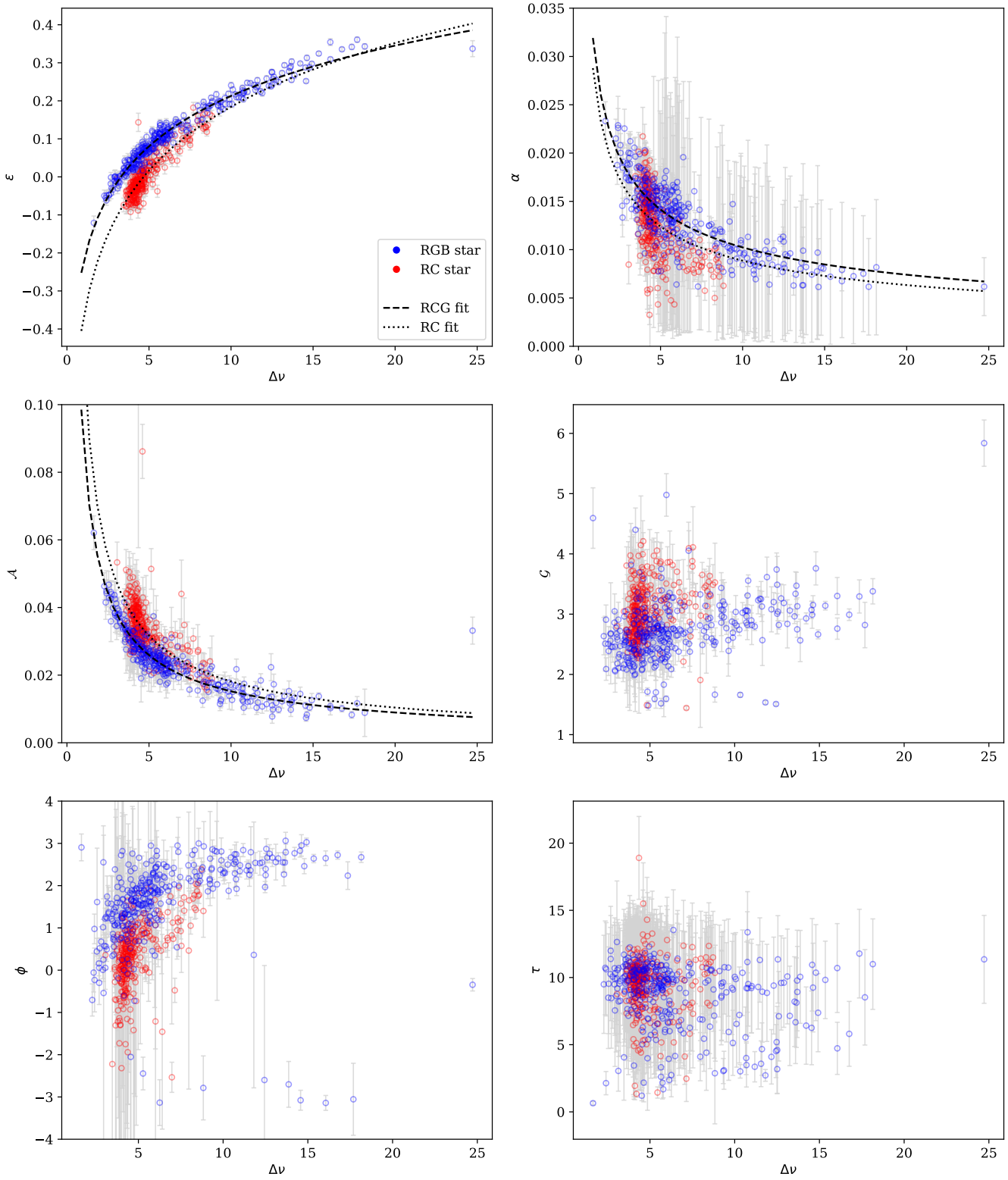

Figure 9: *A range of model parameters are plotted against $\Delta\nu$ (μHz) for the full range of our data from the APOKASC catalogue. Using the Ellsworth classification scheme, Red Giant stars have been coloured blue, with members of the Red Clump in red. For the three parameters (ε, α & $\mathcal{A}$) where we introduced hierarchical elements, the estimated power law has also been plotted.*

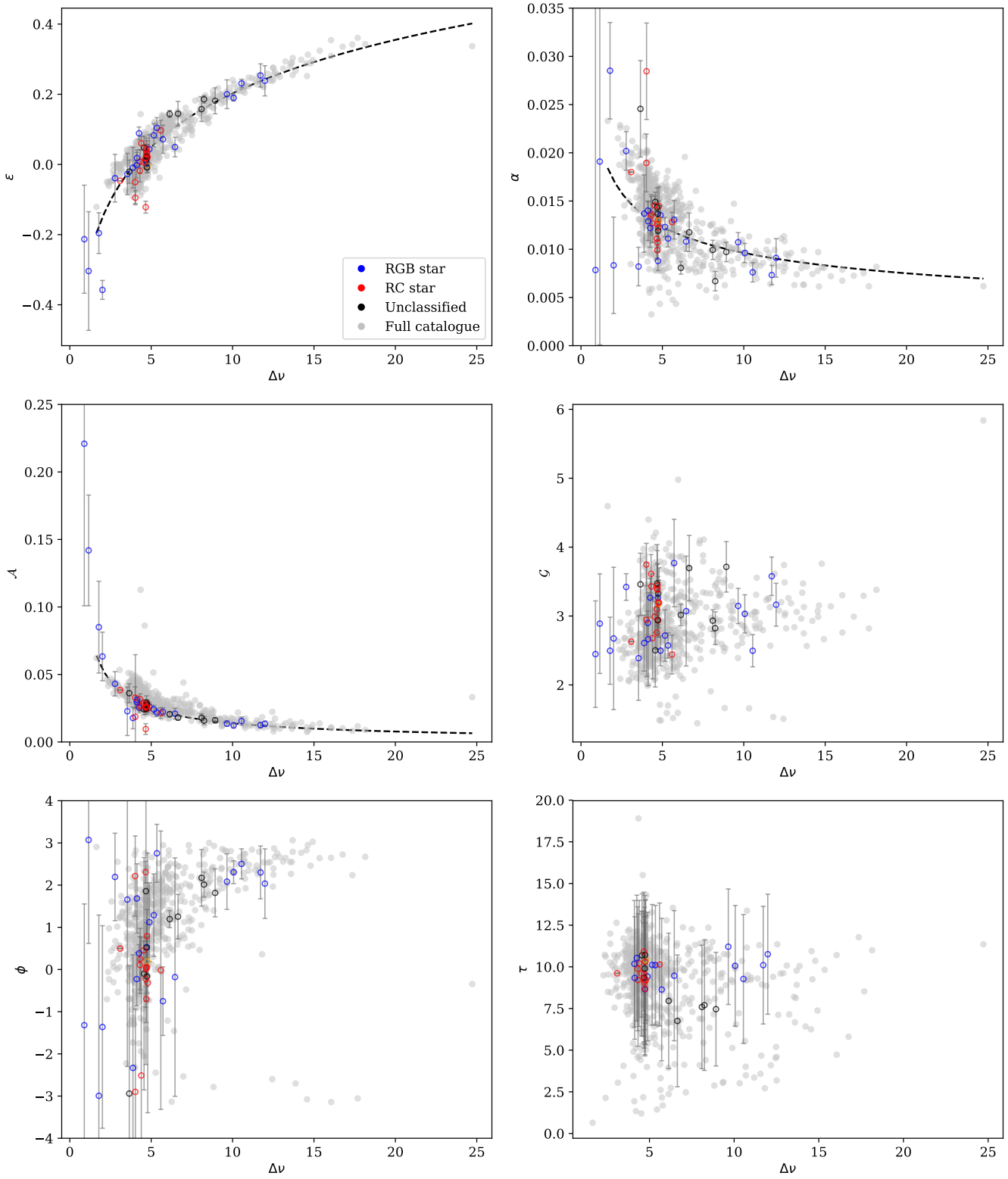

Figure 10: *An equivalent parameter plot for the cluster NGC6819, showing the modelled stars against a background of the previously fitted field stars of the APOKASC catalogue. Again, stars have been classified according to the Elsworth scheme.*

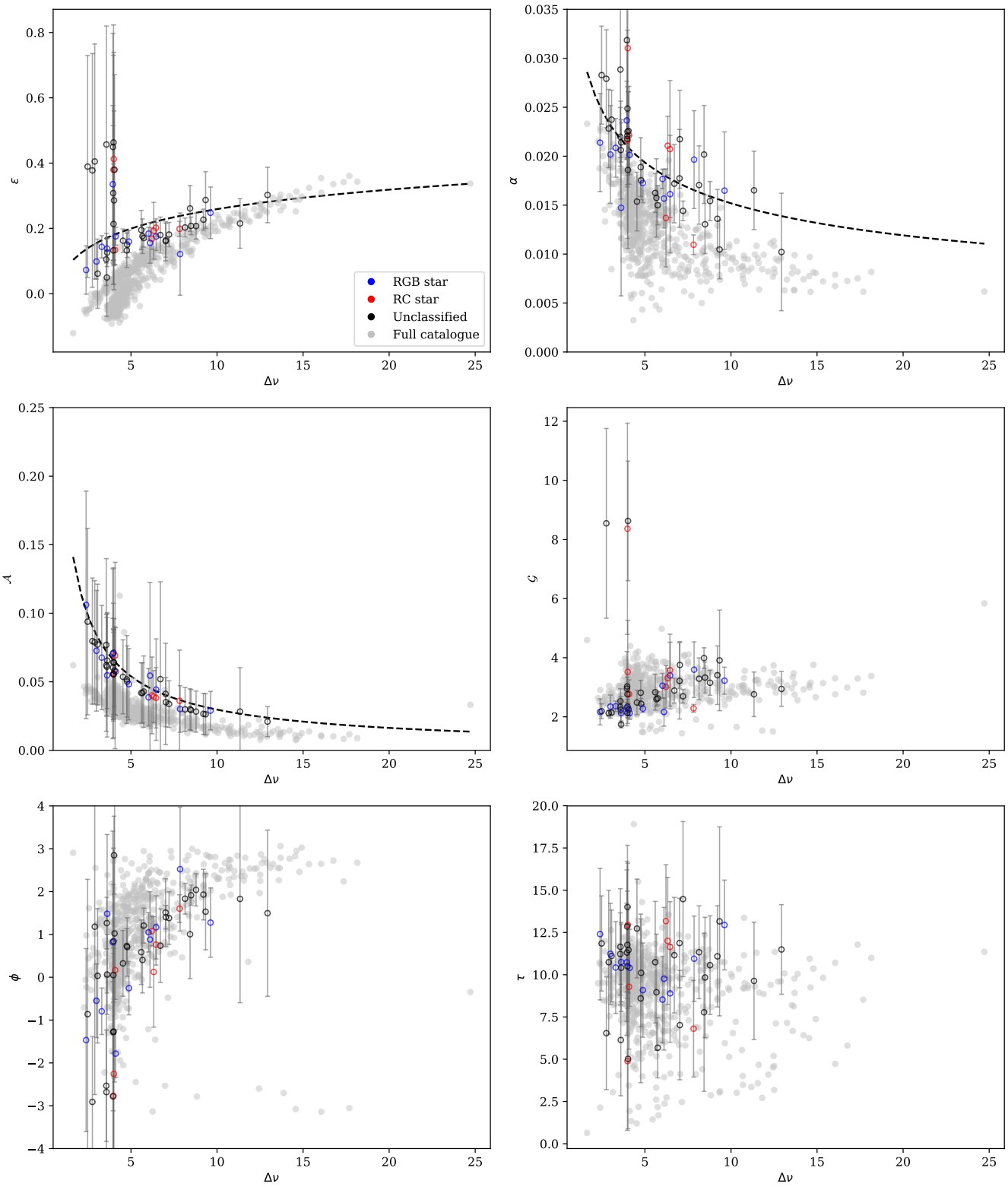

Figure 11: *Again, an equivalent parameter plot for the cluster NGC6719, showing the modelled stars against a background of the previously fitted field stars of the APOKASC catalogue. Again, stars have been classified according to the Elsworth scheme; the majority of the clusters members appear however to have not been classified at this point. Note also the differing power laws derived with the hierarchical parameters.*

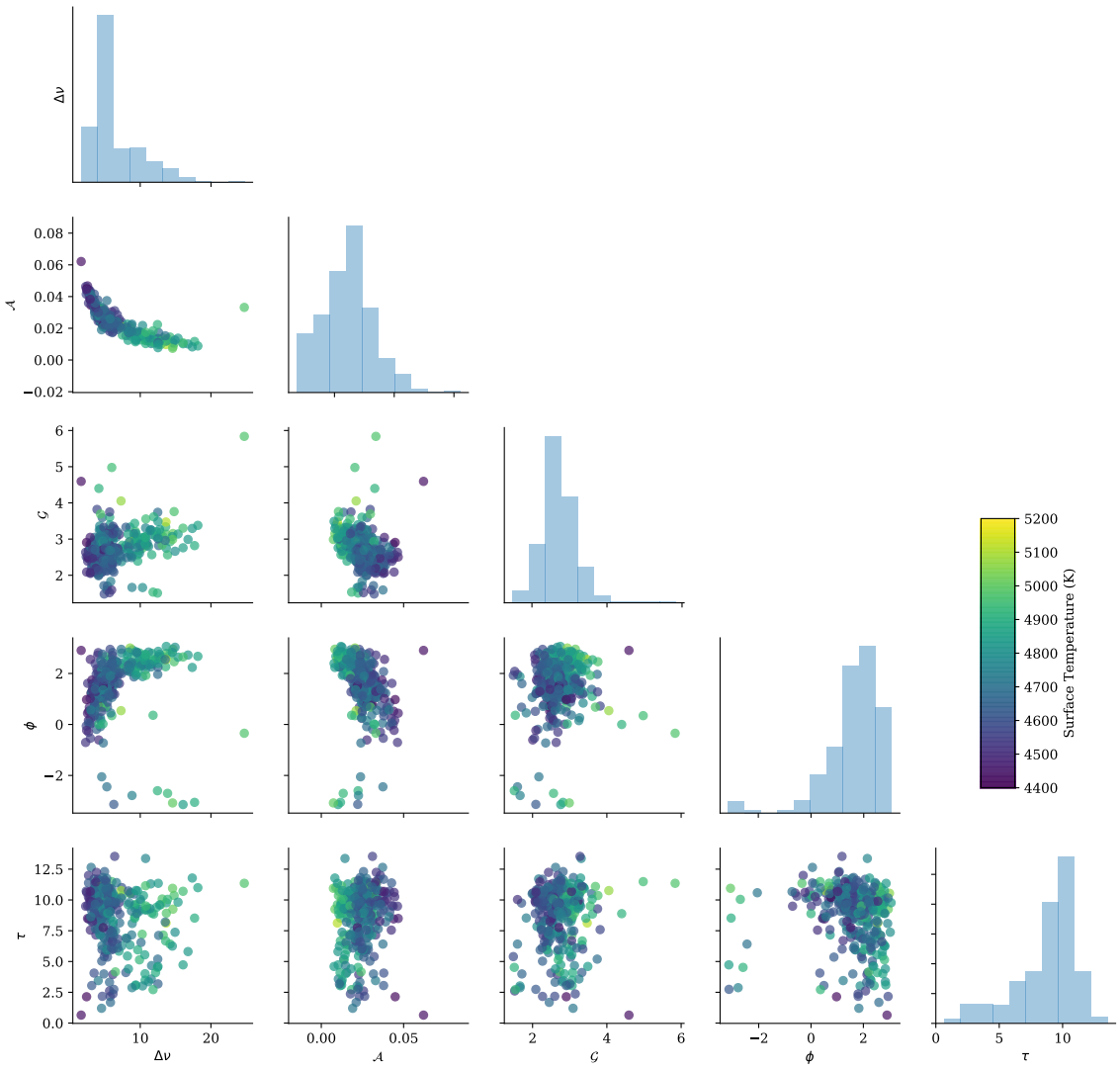

Figure 12: *A correlation diagram for the glitch parameters $\mathcal{A}, \mathcal{G}, \phi$ and τ, with colours mapped to surface temperatures of the star. Histograms have also been provided for each parameter. The power law between glitch amplitude and $\Delta\nu$ is clearly visible, and also how the temperature has an influence on the glitch amplitude and periods.*

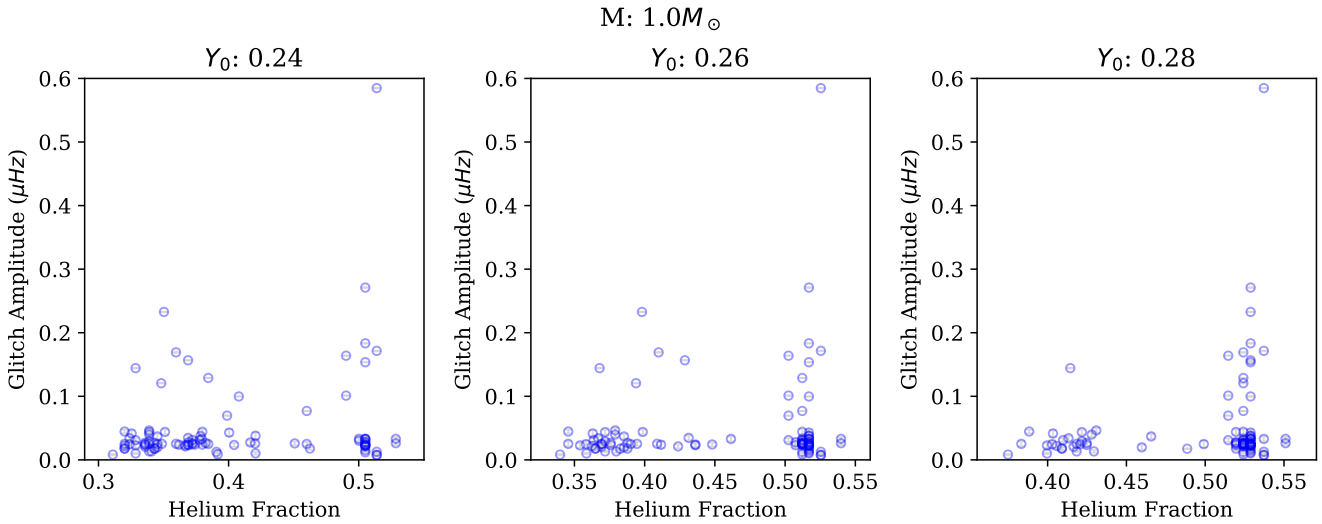

Figure 13: *A comparison of RGB stars fitted using Stan, compared with the closest fitting model provided by MESA and GYRE. The helium fraction along the x-axis represents the current value of helium.*

6 Discussion

6.1 The Hierarchical Glitch

Figure 9 goes a large way to expressing the success of our hierarchical model for the helium glitch. Convergence for both the RGB and RC was excellent ($\hat{R} < 1.01$), strongly indicating that the solutions had been optimised. The data cleanly fits the power laws that were derived with only a couple of apparent outliers, which are summarised in Table 2 showing the asymptotic parameter relations. Errors were only listed for the glitch amplitude relation in Vrard et al. (2015)[2], however we have been able to reduce the error compared to their results; indeed the errors for all the hierarchical parameters are appreciably small compared to the mean value. It is worth noting the relation for the period, $\mathcal{G}$, did not change since we did not intend to modify it, whilst we also introduced an approximate power law in ϕ to help overall convergence. The phase diagram in Figure 9 erroneously appears to show outliers for RGB stars with very low phase values. One must remember however that due to the periodic behaviour of the sinusoidal glitch, $\phi = -\pi \equiv \pi$ so these stars do indeed fit close to the bulk of the RGB stars.

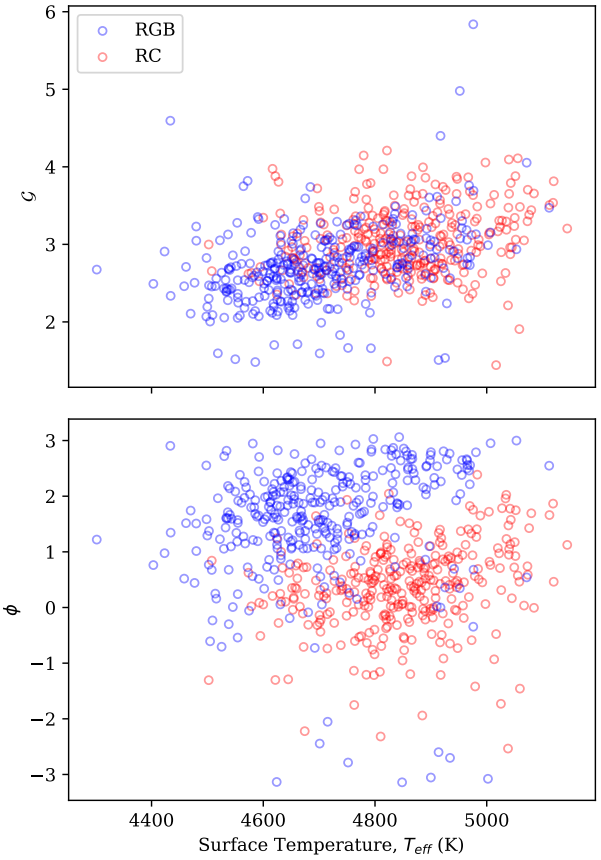

Figure 14: *Dependence of glitch frequency and phase on surface temperature. There is a clear distiction between the two evolutionary phases of stars.*

On the other hand, there are no immediate trends visible with respect to $\langle\Delta\nu\rangle$ for $\mathcal{G}$ or the decay constant τ. One can address this by looking at the correlation plot provided in Figure 12, were surface temperature has been indicated by colour. Now we can see that the glitch amplitude is dependent on both frequency spacing and surface temperature, which follows logically from the notion that as a star evolves up the RGB track, it increases in size. This causes the asymptotic period spacing to decrease, as prescribed in Equation 2; the surface temperature correspondingly cools as the outer envelope expands.

Again, we can check if any parameters in the glitch are not influenced strongly by the frequency spacing: both the glitch period $\mathcal{G}$ and phase ϕ are more strongly dependent on the surface temperature, as shown in Figure 14. On the other hand, the decay parameter τ does not appear to be obviously correlated to anything else. This is an area that could be investigated further in future since it may be dependent on a variable we don't have information on – given the decay is caused by pressure modes becoming comparable in wavelength to the glitch region (as described in Section 2.2), it may be possible to map this to give a 'thickness', as well as its acoustic depth, which can be found using $\mathcal{G}$.[26]

6.2 Open Clusters

Open clusters are groups of gravitationally bound stars that are thought to have formed from the same interstellar cloud. This means that these stars should have negligible differences in their chemical composition and are all the same age. Over time, these usually become unbound and disperse, so the existence of clusters over 1Gyr age provides a useful tool to probe the historical enrichment of stars. NGC6819 is estimated to be 2.5Gyr[27] old whilst NGC6719 is a very unusual cluster with an age of 7.5Gyr and super-solar metallicity.[28]

6.2.1 NGC 6819

Figure 10 provides us with an overview of how stars in the cluster fit in with the general wider population. The cluster appears to fit very well with the hierarchical power law fits in concordance with those previously described in Table 2. The cluster appears to contain a few intermediate-mass stars ($M > 2.0M_{\odot}$) at late stages in their RGB evolution that have swelled to a sigificant size, as shown in Figure 7. These stars have smaller values of $\langle\Delta\nu\rangle$ than any of the population stars, which makes confirmation that they fit the power law difficult, although they appear to fit the extrapolated shape. Consideration must be taken for the impact of dredge-up events on the RGB branch. These highly evolved RGB stars will have certainly passed through the RGB bump which can result in the mixing of the stellar interior, enriching the outer envelope. The introduction of more helium will as described in Section 2.2 raise the amplitude of the helium glitch signal $\mathcal{A}$.

6.2.2 NGC 6791

Conversely, the results for NGC6791 do not align with the population hierarchical parameters, only supporting the cluster's status as an outlier in stellar enrichment theory. For the three hierarchical relations, the cluster forms its own power laws, as seen in Figure 11 – since the three remaining subplots (with respect to glitch period, phase and decay) show the stars falling mostly within the field population, this suggests that it is not simply a poor set of results, rather it may be the cluster that is the cause of the difference.

Arguably the most interesting feature is the relationship for the amplitude, which sits consistently above any values from either the field stars or NGC6819 for a given large frequency spacing. Whilst the error bars are larger than the previous two data sets, this is likely since Stan took longer to converge on values, since they were more distant from those predicted by the hierarchical hyperpriors.

Nonetheless, the consistent increase in the glitch amplitude would be strongly suggestive of a cluster whose members are relatively enriched with helium, which is futher supported by the knowledge that it is a very metal-rich cluster.

A Helium Enrichment Problem?

Why does a cluster such as NGC6791 pose so many problems for our understanding of the chemo-evolution of the galaxy? The answer comes from considering the processes that can influence the amount of helium in the interstellar medium at the point of star formation. The initial helium abundance in the universe is set by the Big Bang and the process of nucleosynthesis, which provided a primordial value of $Y_P \approx 0.24$; since then processes have occurred to enrich the universe, primarily:

- **Type 1a Supernovae** - these occur when a white dwarf progenitor in a binary system exceeds the Chandrasekhar Limit, having accreted

sufficient matter from its companion star. Helium is scattered into the interstellar medium by a violent runaway thermonuclear explosion.

- **ABG Stars** - the asymptotic giant branch is the final stage of evolution for low mass ($M \lessapprox 3M_\odot$) stars. Their internal structure is unstable over long periods; gradually thermal pulses slough off the outer layers (additionally enriched in helium by *s*-process nuclear reactions) into space, enriching the surrounding region.

Contrary to intuition, Type II supernovae are not significant sources of He since their highly explosive nature destroys most of the helium that remained in the star, which was already depleted, having been used in nuclear reactions to form heavier elements.

This means that over many eons, the helium abundance should gradually increase with time – stars that form near galactic cores will also have higher values of Y_0 since there has been greater enrichment from the population. Hence the high metallicity of NGC6791 makes it a target of interest; our models appear to confirm that the cluster is also highly enriched in helium.

6.3 Spread of Abundance

Our current understanding of chemo-evolutionary theory for stars does not provide much allowance for a spread in the helium abundance. Nonetheless, we were able to leverage the power of our hierarchical model to provide us with a measure of the spread for the glitch amplitudes amongst different populations we have been studying, since this will provide and effective proxy for helium abundance.

The results of this analysis are shown in Figure 15. One can see that the largest spread is in the values for the RGB and RC field stars – assuming our statement from the previous paragraph we would expect the clusters to have the same value (corresponding to standard deviation A_σ). It is clear that this is not the case, with the value for NGC6791 approximately 2×10^{-4}, so 20 times smaller than the field value. The result for NGC6819 is also smaller however only marginally; this result also appears to have a high variance which could potentially be attributed to a non-cluster member appearing in the data set, which happened to be in the line of sight of the observation. If this star was significantly different in composition to the cluster, this could cause such a disparity in the data.

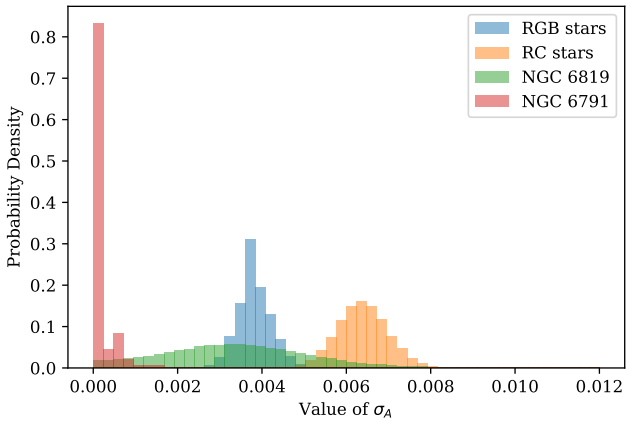

Figure 15: *Comparison of the spread of estimated values of glitch amplitude $\mathcal{A}$ across the different sample populations. Histograms have been normalised such that the probability density sums to one to allow reasonable comparison by eye.*

6.4 Comparing to Models

Having produced a grid of models and series of theoretical oscillation frequencies, we attempted to see if some of the stars fit using Stan could be cross-referenced with these models to estimate an initial helium abundance. In practice, it proved difficult to be able to do this reliably, however Figure 13 shows an example of matching a sample of 1 solar mass stars to their nearest models. As expected from the asymptotic relation for $\mathcal{A}$, the majority of stars fit models with lower amplitudes. However as the initial helium fraction is increased to $Y = 0.28$, a greater number of stars began to match models where the glitch amplitude was larger, as would be expected for a higher helium content.

Whilst we did not have sufficient time to be able to develop and refine this technique into a justified enrichment law, it should provide a useful ground point for a more detailed investigation that could allow an empirical law to be derived. Using a finer grid of parameters in the MESA models with the use of some interpolation technique would probably prove very useful in matching a star to a particular model and hence initial helium fraction.

7 Conclusion

Using a two stage hierarchical model, we were able to correctly estimate the radial oscillation frequencies of a large number of stars from the APOKASC catalogue, as well as derive improved asymptotic parameter relationships for the variables ϵ, α and most importantly the glitch amplitude $\mathcal{A}$ given

$$\mathcal{A} = \begin{cases} (0.089 \pm 0.005)\,\langle\Delta\nu\rangle^{-0.767\pm0.028}, & \text{if RGB} \\ (0.115 \pm 0.007)\,\langle\Delta\nu\rangle^{-0.802\pm0.040}, & \text{if RC.} \end{cases} \tag{14}$$

We were also able to test for any significant correlations between the glitch parameters, including our newly introduced decay parameter – we expect there is some dependence on the radial extent of the glitch however such information was not available at the time. In addition we were able to fit two cluster populations and compare them to the laws provided by our hierarchical model. Whilst NGC6819 broadly followed the existing relationship well, NGC6791 exhibited a uniform inflation of the glitch amplitude that was not consistent with the previously derived power law. Analysis suggests that this could be attributed to a very high helium enrichment in the cluster, which would compliment its already understood metallicity, but further mark the cluster as one that doesn't fit stellar enrichment models.

Finally we were able to assess for spread of helium content amongst the population data. In the closing remarks of their study, Vrard et al. (2015) [2] stated the following:

> *"Even if extracting any direct information on the helium content is certainly very difficult, this work opens the way for testing the second helium ionization zone in a large set of stars with ensemble asteroseismology."*

Using our hierarchical approach, we were able to leverage the power of the population to show that there appears to be a defined spread in the helium enrichment amongst stars, with the spread in NGC691 approximately 20 times smaller than the field population. Whilst tentative at this point, this could offer an important breakthough in the understanding of galactic chemo-evolution and stellar enrichment. Lack of time and theoretical investigation meant we weren't able to pin down an explicit law on enrichment, however the use of stellar models (and a more effective way of comparing with them such as interpolation) could offer a means to extract such values in a future study.

Acknowledgements

Special thanks must be given to Guy Davies as project supervisor, for putting up with our silly questions and providing ambient music for our meetings; also to Warrick Ball, Oliver Hall and Ben Rendle for their help in understanding aspects of the project, including grappling with Fortran, acyclic diagrams and providing data for allowing direct comparisons with data from NGC clusters. Thanks also to Warrick and David Stopps for allowing access to (ab)use the HiROS and ASR computer clusters for the production of our models and simulations. Not least however I'd like to thank my project partner Josh for helping to make the project as enjoyable as it has been for the past year.

Resources

Details of all the scripts and data used in this project, including those used for hierarchical inference in Stan, can be found in the following GitHub repository: `https://www.github.com/daw538/y4project`

References

[1] Onno Pols. *Stellar Structure and Evolution.* Onno Pols (Online), Accessed Feb 2019.

[2] M. Vrard, B. Mosser, C. Barban, K. Belkacem, Y. Elsworth, T. Kallinger, S. Hekker, R. Samadi, and P. G. Beck. Helium signature in red giant oscillation patterns observed bykepler. *Astronomy & Astrophysics*, 579:A84, Jul 2015.

[3] William J. Chaplin and Andrea Miglio. Asteroseismology of solar-type and red-giant stars. *Annual Review of Astronomy and Astrophysics*, 51(1):353–392, Aug 18, 2013.

[4] A.-M. Broomhall, B. Miller, G. R. Davies, S. J. Hale, Y. Elsworth, W. J. Chaplin, R. New, and S. T. Fletcher. Definitive Sun-as-a-star p-mode frequencies: 23 years of BiSON observations. *Monthly Notices of the Royal Astronomical Society: Letters*, 396(1):L100–L104, 06 2009.

[5] S. J. Hale, R. Howe, W. J. Chaplin, G. R. Davies, and Y. P. Elsworth. Performance of the birmingham solar-oscillations network (bison). *Solar Physics*, 291(1):1–28, Jan 2016.

[6] F. Carrier A. Miglio, J. Montalbán. Evidence for a sharp structure variation inside a red-giant star. *Astronomy and Astrophysics*, 520(20):1–4, Sep 2010.

[7] G. Houdek and D. O. Gough. An asteroseismic signature of helium ionization. *Monthly Notices of the Royal Astronomical Society*, 375(3):861–880, 2007.

[8] Kuldeep Verma, H. M. Antia, Sarbani Basu, and Anwesh Mazumdar. A theoretical study of acoustic glitches in low-mass main-sequence stars. *The Astrophysical Journal*, 794(2):114, Sep 30, 2014.

[9] Kuldeep Verma, Keyuri Raodeo, H. M. Antia, Anwesh Mazumdar, Sarbani Basu, Mikkel N. Lund, and Víctor Silva Aguirre. Seismic measurement of the locations of the base of convection zone and helium ionization zone for stars in the *kepler* seismic legacy sample. *MNRAS*, Jan 31, 2017.

[10] G. Houdek and D. O. Gough. An asteroseismic signature of helium ionization. *Monthly Notices of the Royal Astronomical Society*, 375(3):861–880, 2007.

[11] Franz-Ludwig Deubner, Jørgen Christensen-Dalsgaard, and Don Kurtz. *New Eyes to See Inside the Sun and Stars*, volume 185. Springer Netherlands, Dordrecht, Netherlands, 1 edition, 1998.

[12] Bob Carpenter, Andrew Gelman, Matthew Hoffman, Daniel Lee, Ben Goodrich, Michael Betancourt, Marcus Brubaker, Jiqiang Guo, Peter Li, and Allen Riddell. Stan: A probabilistic programming language. *Journal of Statistical Software, Articles*, 76(1):1–32, 2017.

[13] Marc Pinsonneault, Yvonne Elsworth, Courtney Epstein, Saskia Hekker, Sz Mészáros, William J. Chaplin, Jennifer A. Johnson, R García, Jon Holtzman, Savita Mathur, Ana Garcia Perez, Victor Silva Aguirre, Léo Girardi, Sarbani Basu, Matthew Shetrone, Dennis Stello, Carlos Allende Prieto, Deokkeun An, Paul Beck, and Gail Zasowski. The apokasc catalog: An asteroseismic and spectroscopic joint survey of targets in the kepler fields. *The Astrophysical Journal Supplement Series*, 215, 10 2014.

[14] Yvonne Elsworth, Saskia Hekker, Sarbani Basu, and Guy R. Davies. A new method for the asteroseismic determination of the evolutionary state of red-giant stars. *Monthly Notices of the Royal Astronomical Society*, 466(3):3344–3352, Apr 21, 2017.

[15] A. M Broomhall, A. Miglio, J. Montalbán, P. Eggenberger, W. J. Chaplin, Y. Elsworth, R. Scuflaire, P. Ventura, and G. A. Verner. Prospects for asteroseismic inference on the envelope helium abundance in red giant stars. *Monthly Notices of the Royal Astronomical Society*, 440(2):1828–1843, May 11, 2014.

[16] Marc H. Pinsonneault and Yvonne P. Elsworth et al. The second apokasc catalog: The empirical approach. *The Astrophysical Journal Supplement Series*, 239(2):32, Dec 10, 2018.

[17] B. Paxton, L. Bildsten, A. Dotter, F. Herwig, P. Lesaffre, and F. Timmes. Modules for Experiments in Stellar Astrophysics (MESA). , 192:3, jan 2011.

[18] B. Paxton, M. Cantiello, P. Arras, L. Bildsten, E.F. Brown, A. Dotter, C. Mankovich, M.H. Montgomery, D. Stello, F.X. Timmes, and R. Townsend. Modules for Experiments in Stellar Astrophysics (MESA): Planets, Oscillations, Rotation, and Massive Stars. , 208:4, sep 2013.

[19] B. Paxton, P. Marchant, J. Schwab, E. B. Bauer, L. Bildsten, M. Cantiello, L. Dessart, R. Farmer, H. Hu, N. Langer, R. H. D. Townsend, D. M. Townsley, and F. X. Timmes. Modules for Experiments in Stellar Astrophysics (MESA): Binaries, Pulsations, and Explosions. , 220:15, sep 2015.

[20] B. Paxton, J. Schwab, E. B. Bauer, L. Bildsten, S. Blinnikov, P. Duffell, R. Farmer, J. A. Goldberg, P. Marchant, E. Sorokina, A. Thoul, R. H. D. Townsend, and F. X. Timmes. Modules for Experiments in Stellar Astrophysics (MESA): Convective Boundaries, Element Diffusion, and Massive Star Explosions. , 234:34, feb 2018.

[21] R. H. D. Townsend and S. A. Teitler. gyre: an open-source stellar oscillation code based on a new magnus multiple shooting scheme. *Monthly Notices of the Royal Astronomical Society*, 435(4):3406–3418, Nov 11, 2013.

[22] R. H. D. Townsend, J. Goldstein, and E. G. Zweibel. Angular momentum transport by heat-driven g-modes in slowly pulsating b stars. *Monthly Notices of the Royal Astronomical Society*, 475(1):879–893, Mar 21, 2018.

[23] D. R. Reese. AIMS: Asteroseismic Inference on a Massive Scale. Astrophysics Source Code Library, November 2016.

[24] Mikkel N. Lund and Daniel R. Reese. Asteroseismic stellar modelling with aims. *Solar and Stellar Astrophysics*, Nov 6, 2017.

[25] Ben M. Rendle, Gaël Buldgen, Andrea Miglio, Daniel Reese, Arlette Noels, Guy R. Davies, Tiago L. Campante, William J. Chaplin, Mikkel N. Lund, James S. Kuszlewicz, Laura J. A. Scott, Richard Scuflaire, Warrick H. Ball, Jiri Smetana, and Benard Nsamba. aims – a new tool for stellar parameter determinations using asteroseismic constraints. *Monthly Notices of the Royal Astronomical Society*, 484(1):771–786, Mar 21, 2019.

[26] A. Mazumdar, M. J. P. F. G Monteiro, J. Ballot, H. M. Antia, S. Basu, G. Houdek, S. Mathur, M. S. Cunha, V. Silva Aguirre, R. A. Garcia, D. Salabert, G. A. Verner, J. Christensen-Dalsgaard, T. S. Metcalfe, D. T. Sanderfer, S. E. Seader, J. C. Smith, and W. J. Chaplin. Measurement of acoustic glitches in solar-type stars from oscillation frequencies observed by kepler. *ASTROPHYSICAL JOURNAL*, 782(1), Dec 17, 2013.

[27] Lauren N. Brewer and Eric L. et al. Sandquist. Determining the age of the kepler open cluster ngc 6819 with a new triple system and other eclipsing binary stars. *Astronomical Journal (Online)*, 151(3), 3 2016.

[28] S. Hardis F. Grundahl, J. V. Clausen and S. Frandsen. A new standard: age and distance for the open cluster ngc 6791 from the eclipsing binary member v20. *Astronomical & Astrophysics*, 492(1), 9 2008.